Supplementary Materials: Exceptional points in oligomer chains

Charles Andrew Downing[1] and Vasil Arkadievich Saroka[2,3]

[1]*Department of Physics and Astronomy, University of Exeter, Exeter EX4 4QL, United Kingdom*
[2]*Center for Quantum Spintronics, Department of Physics, Norwegian University of Science and Technology, NO-7491 Trondheim, Norway*
[3]*Institute for Nuclear Problems, Belarusian State University, Bobruiskaya 11, 220030 Minsk, Belarus*
email: c.a.downing@exeter.ac.uk, vasil.saroka@ntnu.no

In these Supplementary Materials we outline some foundational results for a dimer ($\mathcal{N} = 2$) of oscillators, which provides additional insight into the behaviour of the trimer chain ($\mathcal{N} = 3$) which is considered in the main text. We also provide a treatment of the quadrimer chain ($\mathcal{N} = 4$), which builds further intuition about the physics of general oligomer chains. Finally, using the transfer matrix method, we investigate a general $\mathcal{PT}$-symmetric oligomer chain of size $\mathcal{N}$, leading to some useful neat results.

CONTENTS

I. SUPPLEMENTARY NOTE 1: FOUNDATIONAL RESULTS FOR A DIMER

The Hamiltonian $\hat{H}$ of a pair of oscillators, each of resonance frequency ω_0 and coupled at a strength g, reads

$$\hat{H} = \omega_0 \left(b_1^\dagger b_1 + b_2^\dagger b_2 \right) + g \left(b_1^\dagger b_2 + b_1^\dagger b_2 \right), \tag{S1}$$

where $b_n^\dagger$ (b_n) creates (destroys) a bosonic excitation on the n-th oscillator. The normal modes are associated with the hybridized eigenfrequencies ω_n, where

$$\omega_2 = \omega_0 + g, \tag{S2a}$$
$$\omega_1 = \omega_0 - g, \tag{S2b}$$

revealing a Rabi splitting of $\omega_2 - \omega_1 = 2g$ between the upper and lower energy levels. The quantum master equation describing the open quantum system of the two aforementioned oscillators connected to two heat baths is

$$\partial_t \rho = \mathrm{i}[\rho, \hat{H}] + \sum_{n=1,2} \frac{\gamma_n}{2} \left(2 b_n \rho b_n^\dagger - b_n^\dagger b_n \rho - \rho b_n^\dagger b_n \right) + \sum_{n=1,2} \frac{P_n}{2} \left(2 b_n^\dagger \rho b_n - b_n b_n^\dagger \rho - \rho b_n b_n^\dagger \right), \tag{S3}$$

where γ_n and P_n are four parameters describing incoherent loss from, and gain into, the n-th oscillator.

A. $\mathcal{PT}$ symmetry

In a similar manner to the manipulations leading to Eq. (6) in the main text, the Hamiltonian of Eq. (S1) and master equation of Eq. (S3) lead to the mean-field Schrödinger-like equation

$$\mathrm{i}\partial_t \psi = \mathcal{H} \psi, \tag{S4}$$

where the two-dimensional Bloch vector ψ, and the 2×2 dynamical matrix $\mathcal{H}$, are given by

$$\psi = \begin{pmatrix} \langle b_1 \rangle \\ \langle b_2 \rangle \end{pmatrix}, \qquad \mathcal{H} = \begin{pmatrix} \omega_0 - \mathrm{i}\frac{\Gamma_1}{2} & g \\ g & \omega_0 - \mathrm{i}\frac{\Gamma_2}{2} \end{pmatrix}, \qquad \Gamma_n = \gamma_n - P_n. \tag{S5}$$

This analysis suggests a $\mathcal{PT}$-symmetric setup of the dimer, as sketched in Fig. S1 (a), where the first oscillator only is pumped and the second oscillator exhibits an equivalent loss ($P_1 = \gamma_2 = \kappa$ and $P_2 = \gamma_1 = 0$). This balanced loss and gain arrangement may be described by the non-Hermitian Hamiltonian $\hat{H}'$ [cf. Eq. (S1)]

$$\hat{H}' = \left(\omega_0 + \mathrm{i}\tfrac{\kappa}{2} \right) b_1^\dagger b_1 + \left(\omega_0 - \mathrm{i}\tfrac{\kappa}{2} \right) b_2^\dagger b_2 + g \left(b_1^\dagger b_2 + b_2^\dagger b_3 + \mathrm{h.c.} \right), \tag{S6}$$

such that the reconstructed eigenfrequencies ω_n' read [cf. Eq. (S2)]

$$\omega_2' = \omega_0 + \Omega, \tag{S7a}$$
$$\omega_1' = \omega_0 - \Omega, \tag{S7b}$$

where the renormalized splitting $\omega_2' - \omega_1' = 2\Omega$, in terms of the frequency

$$\Omega = \sqrt{g^2 - \left(\tfrac{\kappa}{2} \right)^2}. \tag{S8}$$

Clearly, the exceptional point marking the border between real and complex eigenfrequencies for this dimer ($\mathcal{N} = 2$) system is located at

$$\left(\frac{g}{\kappa} \right)_{\mathcal{N}=2} = \frac{1}{2}, \tag{S9}$$

as mentioned in Eq. (1) of the main text. The consequences of Eq. (S9) may be observed in Fig. S1 (b) and (c), which plot the real and imaginary parts of ω_n' respectively, using Eq. (S7). Technically, this is an exceptional point of 2nd order because two eigenvalues coalesce at the exceptional point. As we shall see, the existence of this boundary has profound implications for the physics of a pair of coupled oscillators.

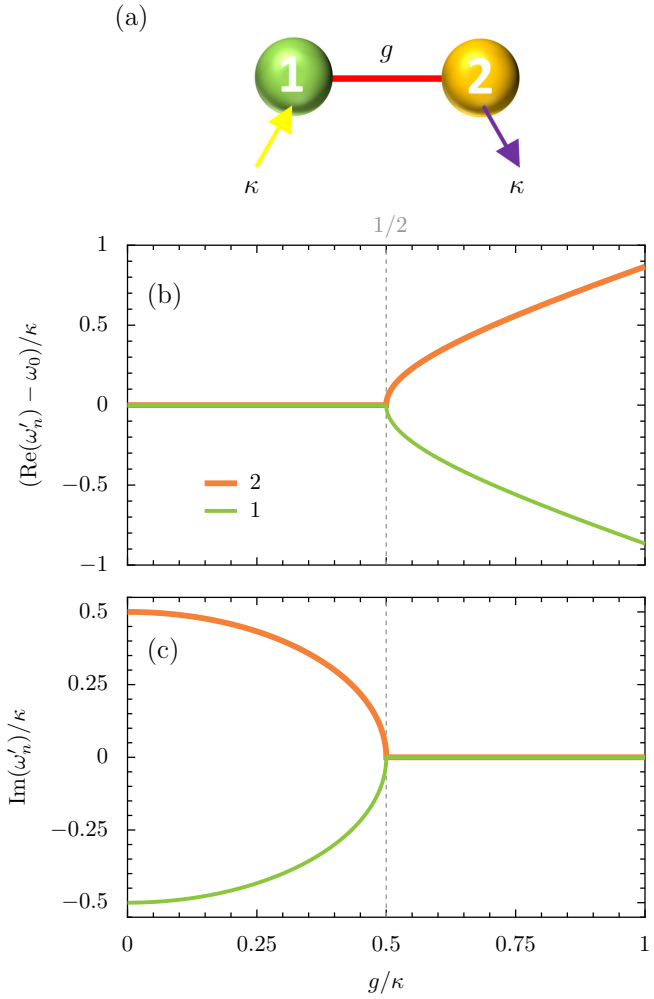

FIG. S1. **$\mathcal{PT}$-symmetric dimer.** Panel (a): a sketch of the $\mathcal{PT}$-symmetric dimer, where each oscillator is of resonance frequency ω_0, and the coupling constant is g. The first oscillator is subject to gain κ (yellow arrow), and the second oscillator to loss κ (purple arrow). Panel (b): the real parts of the eigenfrequencies ω_n' of the dimer, measured from ω_0, as a function of g, in units of κ [cf. Eq. (S7)]. Panel (c): the corresponding imaginary parts of the eigenfrequencies ω_n'. Vertical dashed lines: exceptional point marking broken-unbroken $\mathcal{PT}$ symmetry phases [cf. Eq. (S9)].

B. Dynamics

In an analogous fashion to the calculation leading to Eq. (14) in the main text, the second moments associated with the dimer may be found from Eq. (S3), and can be encapsulated in the following equation of motion

$$\frac{\mathrm{d}}{\mathrm{d}t}\mathbf{u} = \mathbf{P} - \mathbf{M}\mathbf{u}, \tag{S10}$$

where $\mathbf{u}$, which contains the mean populations and coherences, the drive term $\mathbf{P}$ and the 4×4 matrix $\mathbf{M}$ respectively read

$$\mathbf{u} = \begin{pmatrix} \langle b_1^\dagger b_1 \rangle \\ \langle b_2^\dagger b_2 \rangle \\ \langle b_1^\dagger b_2 \rangle \\ \langle b_2^\dagger b_1 \rangle \end{pmatrix}, \qquad \mathbf{P} = \begin{pmatrix} P_1 \\ P_2 \\ 0 \\ 0 \end{pmatrix}, \qquad \mathbf{M} = \begin{pmatrix} \Gamma_1 & 0 & \mathrm{i}g & -\mathrm{i}g \\ 0 & \Gamma_2 & -\mathrm{i}g & \mathrm{i}g \\ \mathrm{i}g & -\mathrm{i}g & \frac{\Gamma_1+\Gamma_2}{2} & 0 \\ -\mathrm{i}g & \mathrm{i}g & 0 & \frac{\Gamma_1+\Gamma_2}{2} \end{pmatrix}, \tag{S11}$$

where Γ_n is defined in Eq. (S5).

In the $\mathcal{PT}$-symmetric arrangement of the dimer, as sketched in Fig. S1 (a), a steady state is not formed and only the transient solution of Eq. (S10) arises. The mean populations $\langle b_1^\dagger b_1 \rangle$ and $\langle b_2^\dagger b_2 \rangle$ of the first oscillator and second oscillator respectively

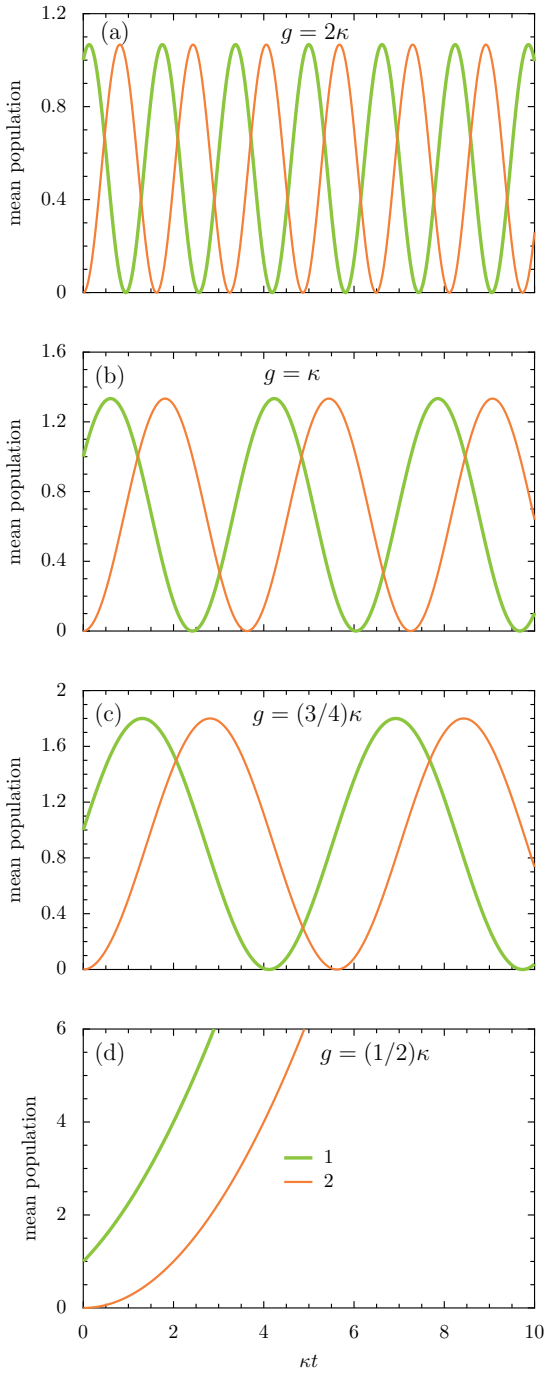

FIG. S2. **Dynamics of the $\mathcal{PT}$-symmetric dimer.** Evolution of the mean populations $\langle b_n^\dagger b_n \rangle$ across the dimer, as a function of time t, in units of the inverse loss-gain parameter κ^{-1} [cf. Eq. (S12) and Eq. (S13)]. The results for the first and second oscillators are denoted by the thick green and thin orange lines respectively [see the legend in panel (d)]. Upon descending the column of panels, the coupling constant g reduces from above to exactly at the exceptional point of $g = \kappa/2$.

may be found analytically as

$$\langle b_1^\dagger b_1 \rangle = \frac{2g^2 - \kappa^2}{4\Omega^2} \cos(2\Omega t) + \frac{\kappa}{2\Omega} \sin(2\Omega t) + \frac{g^2}{2\Omega^2}, \tag{S12a}$$

$$\langle b_2^\dagger b_2 \rangle = \frac{g^2}{2\Omega^2} \Big\{ 1 - \cos(2\Omega t) \Big\}, \tag{S12b}$$

where the frequency Ω is defined in Eq. (S8), and the initial condition at $t = 0$ is $\langle b_1^\dagger b_1 \rangle = 1$ and $\langle b_2^\dagger b_2 \rangle = 0$. The oscillatory

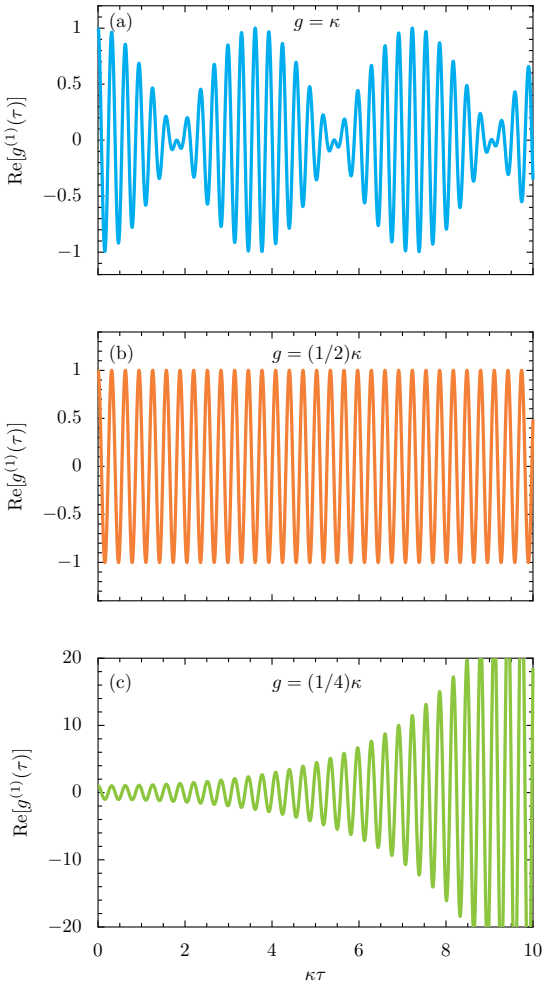

FIG. S3. **Dynamics of the coherence.** Evolution of the real part of the first-order correlation function $g^{(1)}(\tau)$, as a function of the time delay τ, in units of the inverse loss-gain parameter κ^{-1} [cf. Eq. (S17)]. Panel (a)/(b)/(c): the coupling constant g is above/at/below the exceptional point located at $g = \kappa/2$. In the figure, $\omega_0 = 20\kappa$.

dynamics of the populations, as described by Eq. (S12), are plotted in Fig. S2 (a, b, c) for increasingly weak coupling g, which leads to population cycles of increasingly large amplitude and long wavelength. Below the exceptional point at $g = \kappa/2$, Eq. (S12) transforms into the exponentially increasing mean populations

$$\langle b_1^\dagger b_1\rangle = \frac{\kappa^2 - 2g^2}{4\Upsilon^2}\cosh(2\Upsilon t) + \frac{\kappa}{2\Upsilon}\sinh(2\Upsilon t) - \frac{g^2}{2\Upsilon^2}, \tag{S13a}$$

$$\langle b_2^\dagger b_2\rangle = \frac{g^2}{2\Upsilon^2}\Big\{\cosh(2\Upsilon t) - 1\Big\}, \tag{S13b}$$

where we have introduced the frequency [cf. Eq. (S8)]

$$\Upsilon = \sqrt{\left(\tfrac{\kappa}{2}\right)^2 - g^2}. \tag{S14}$$

Typical growing populations are displayed in Fig. S2 (d), where upon approaching the exceptional point $g \to \kappa/2$ quadratic relations are obtained from Eq. (S13): $\langle b_1^\dagger b_1\rangle \to (1+\kappa t/2)^2$ and $\langle b_2^\dagger b_2\rangle \to (\kappa t/2)^2$. The fundamental features shown in Fig. S1 and Fig. S2 complement the results in the main text for longer chains.

C. Correlations

The temporal coherence in the dimer can be quantified through the first-order correlation function $g^{(1)}(\tau)$, defined via

$$g^{(1)}(\tau) = \lim_{t\to\infty} \frac{\langle b^\dagger(t) b(t+\tau)\rangle}{\langle b^\dagger(t) b(t)\rangle}, \tag{S15}$$

with τ the delay time, and for some operator b. For a single driven-dissipative oscillator, one finds $g^{(1)}(\tau) = \mathrm{e}^{-\mathrm{i}\omega_0\tau}\mathrm{e}^{-(\gamma-P)\tau/2}$, that is a fast oscillating function of τ, with the factor $\gamma - P$ determining the coherence time. Crucially, the maximum coherence found at zero delay $|g^{(1)}(0)| = 1$, is damped exponentially towards complete incoherence $|g^{(1)}(\infty)| = 0$ at large timescales, due to the increased chances for phase randomness with long delay times.

In the style of the derivation leading to Eq. (22) in the main text, the two-time correlator of interest $\langle b_1^\dagger(t) b_1(t+\tau)\rangle$ may be found from Eq. (S3), leading to the equation of motion

$$\partial_\tau \mathbf{v} + \mathbf{Q}\mathbf{v} = 0, \qquad \mathbf{v} = \begin{pmatrix} \langle b_1^\dagger(t) b_1(t+\tau)\rangle \\ \langle b_1^\dagger(t) b_2(t+\tau)\rangle \end{pmatrix}, \qquad \mathbf{Q} = \begin{pmatrix} \mathrm{i}\omega_0 + \frac{\Gamma_1}{2} & \mathrm{i}g \\ \mathrm{i}g & \mathrm{i}\omega_0 + \frac{\Gamma_2}{2} \end{pmatrix}, \tag{S16}$$

where Γ_n is given by Eq. (S5). A similar equation may be found for $\langle b_2^\dagger(t) b_2(t+\tau)\rangle$.

The $\mathcal{PT}$-symmetric setup of the dimer, as displayed in Fig. S1 (a), along with the definition of Eq. (S15) and the solution to Eq. (S16), leads to the simple expressions for the first-order correlation function

$$g^{(1)}(\tau) = \begin{cases} \mathrm{e}^{-\mathrm{i}\omega_0\tau}\cos(\Omega\tau), & g > \kappa/2, \\ \mathrm{e}^{-\mathrm{i}\omega_0\tau}, & g = \kappa/2, \\ \mathrm{e}^{-\mathrm{i}\omega_0\tau}\cosh(\Upsilon\tau), & g < \kappa/2, \end{cases} \tag{S17}$$

which holds for both the first and second oscillator [with the operator b_1 or b_2 used in Eq. (S15)]. This result reveals the importance of the exceptional point, which borders oscillatory and divergent behaviours of the first-order coherence function. We plot the real part of the first-order correlation function $g^{(1)}(\tau)$, as a function of the time delay τ, in Fig. S3 using Eq. (S17), illustrating partial coherence in panel (a), perfect coherence in panel (b), and a broken $\mathcal{PT}$-symmetric phase induced divergence in panel (c).

II. SUPPLEMENTARY NOTE 2: THE QUADRIMER CHAIN

Here we look at simplest nontrivial chain with an even number of oscillators, the quadrimer chain ($\mathcal{N} = 4$). Directly from the quadrimer Hamiltonian, which is a natural extension of Eq. (2) in the main text, the four eigenfrequencies ω_n are

$$\omega_{4,1} = \omega_0 \pm \left(\tfrac{\sqrt{5}+1}{2}\right) g, \tag{S18a}$$

$$\omega_{3,2} = \omega_0 \pm \left(\tfrac{\sqrt{5}-1}{2}\right) g, \tag{S18b}$$

which also arise from the general formula of Eq. (28) in the main text with $\mathcal{N} = 4$.

A. $\mathcal{PT}$ symmetry

Let us consider the $\mathcal{PT}$ symmetric setup of the quadrimer chain, as sketched in Fig. S4 (a). The system is invariant under the necessary twin transformations $\mathrm{i} \to -\mathrm{i}$ and $(1,2,3,4) \to (4,3,2,1)$, flipping time and space. The resulting eigenfrequencies ω_n' are

$$\omega_{4,1}' = \omega_0 \pm \tfrac{1}{2\sqrt{2}}\sqrt{12g^2 - \kappa^2 + \mu^2}, \tag{S19a}$$

$$\omega_{3,2}' = \omega_0 \pm \tfrac{1}{2}\sqrt{6g^2 - \tfrac{\kappa^2}{2} - \tfrac{\mu^2}{2}}, \tag{S19b}$$

where we have introduced the quantity

$$\mu^2 = \sqrt{80g^4 - 8g^2\kappa^2 + \kappa^4}. \tag{S20}$$

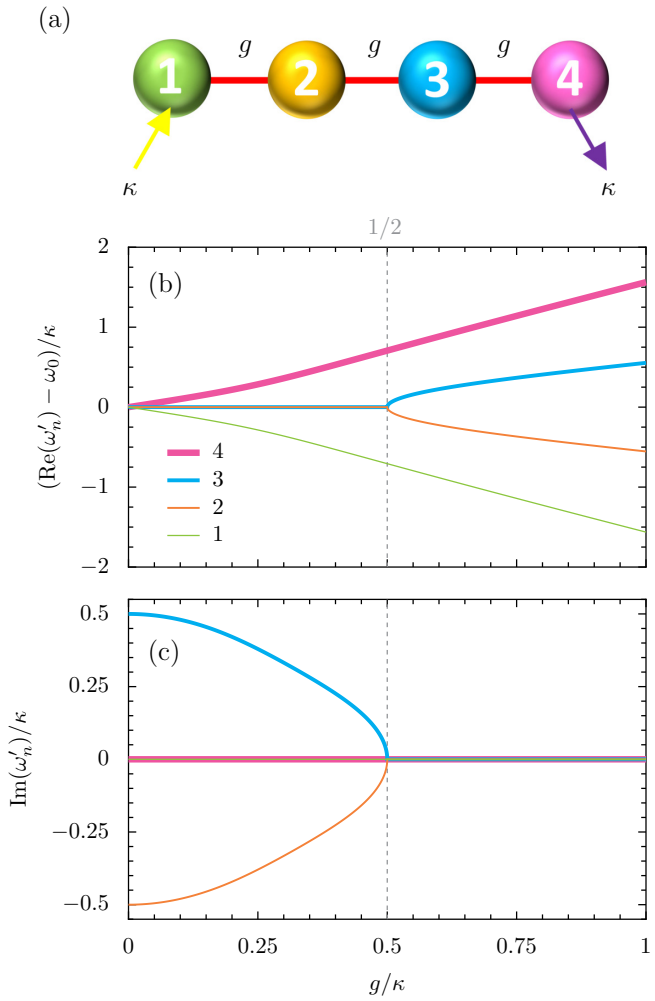

FIG. S4. **$\mathcal{PT}$-symmetric quadrimer.** Panel (a): a sketch of the $\mathcal{PT}$-symmetric quadrimer chain, where each oscillator is of resonance frequency ω_0, and the coupling constant is g. The first oscillator is subject to gain κ (yellow arrow), and the final oscillator to loss κ (purple arrow). Panel (b): the real parts of the eigenfrequencies ω_n' of the trimer, measured from ω_0, as a function of g, in units of κ [cf. Eq. (S19)]. Panel (c): the corresponding imaginary parts of the eigenfrequencies ω_n'. Vertical dashed lines: exceptional point marking broken-unbroken $\mathcal{PT}$ symmetry phases [cf. Eq. (S21)].

Like the celebrated dimer ($\mathcal{N} = 2$), and in fact all oligomers with a even number of sites [cf. Fig. 6 in the main text], the exceptional point arises at

$$\left(\frac{g}{\kappa}\right)_{\mathcal{N}=4} = \frac{1}{2}. \tag{S21}$$

We plot the eigenfrequencies ω_n' of Eq. (S19) in Fig. S4, where the real [imaginary] parts are displayed in panel (b) [(c)], and the exceptional point of Eq. (S21) is denoted by the dashed gray lines. As for the dimer, and indeed for any even-length oligomer in this $\mathcal{PT}$ arrangement, the exceptional point is rather conventional, being 2nd order (since only two eigenvalues coalesce).

B. Long-range coupling

We investigate effects beyond nearest-neighbor coupling by adding second-neighbor coupling h to the system, as sketched in Fig. S5 (a). In this way, the coupled modes can be thought of as belonging to two coupled rings, or to a chain with long-range interactions. This coupling extension generalizes the eigenfrequencies ω_n of Eq. (S18) to $\tilde{\omega}_n$, where

$$\tilde{\omega}_{4,1} = \omega_0 \pm \tfrac{1}{2}\sqrt{5g^2 \pm 8gh + 4h^2} \pm \tfrac{g}{2}, \tag{S22a}$$

$$\tilde{\omega}_{3,2} = \omega_0 \mp \tfrac{1}{2}\sqrt{5g^2 \mp 8gh + 4h^2} \mp \tfrac{g}{2}. \tag{S22b}$$

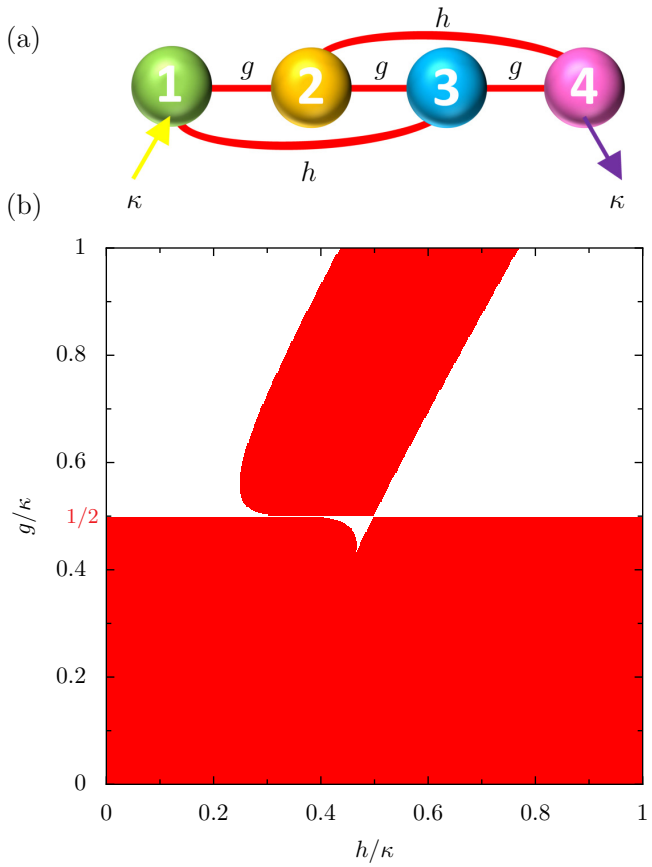

FIG. S5. **Long-range coupling in the quadrimer.** Panel (a): a sketch of the $\mathcal{PT}$-symmetric quadrimer chain beyond nearest-neighbor coupling, where the first(second)-neighbor coupling constant is g (h). The first oscillator is subject to gain κ (yellow arrow), and the final oscillator to loss κ (purple arrow). Panel (b): the $\mathcal{PT}$ symmetry phase diagram of the quadrimer chain, given by the evolution of the exceptional point $(g/\kappa)_4$ with the first and second-neighbor couplings, both in units of κ. Red: broken phase. White: unbroken phase.

In the $\mathcal{PT}$ arrangement of the quadrimer, as presented in Fig. S5 (a), the eigenfrequencies $\tilde{\omega}'_n$ are analytic but are too unwieldy to be given here. However, they give rise to the phase diagram sketched in Fig. S5 (b), which shows the regions of unbroken (white) and broken (red) $\mathcal{PT}$ symmetry, as a function of the first and second neighbor coupling constants g and h. The structure of these domains is noticeably richer than in the trimer case of Fig. 4 (b) in the main text, and includes an interesting enclave of unbroken phase domain near to $h = \kappa/2$. Furthermore, now the equal coupling case ($h = g$, diagonal across the panel) allows for both broken and unbroken $\mathcal{PT}$-symmetric phases, in stark contrast to the trimer case of the main text.

We complement the complex structure of the phase diagram in Fig. S5 (b) by taking cuts in the phase diagram at $h = 0.1\kappa, 0.3\kappa, 0.45\kappa, 0.5\kappa, 0.6\kappa$ and 0.8κ, which results in Fig. S6, where h increases from left to right across the row of five columns. The upper panels of Fig. S6 show the real parts of the eigenfrequencies $\tilde{\omega}'_n$, while the lower panels display the corresponding imaginary parts. The vertical dashed lines mark the exceptional points, which provide more insight into the governing phase diagram, including making explicit that the exceptional points are of 2nd order.

III. SUPPLEMENTARY NOTE 3: ON GENERAL OLIGOMER CHAINS

.

Here we employ the transfer matrix method in our consideration of a general $\mathcal{PT}$-symmetric oligomer chain of an arbitrary size $\mathcal{N}$. In doing so, we derive Eq. (29) from the main text, which describes the evolution of the location of the exceptional point $(g/\kappa)_\mathcal{N}$ with the system size $\mathcal{N}$.

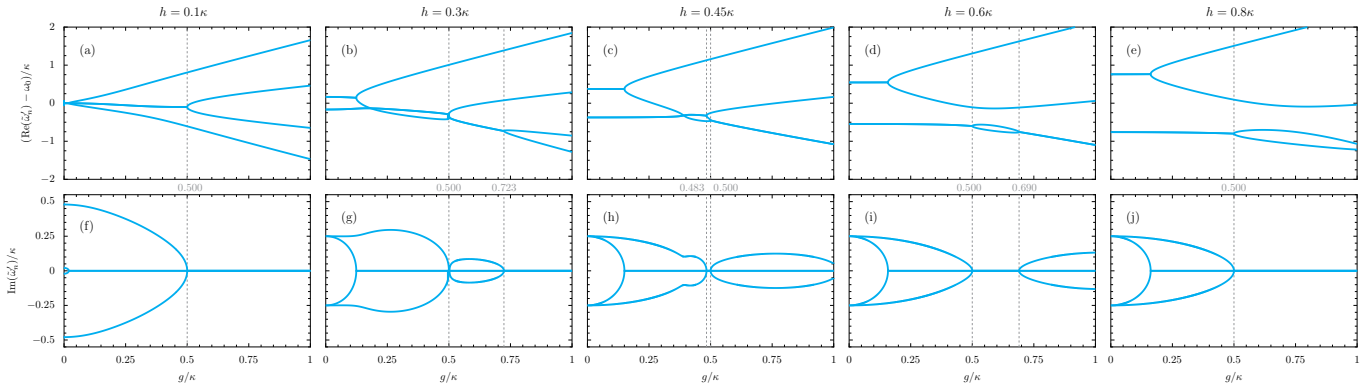

FIG. S6. **Exceptional points in the quadrimer with long-range coupling.** Upper panels: the real parts of the eigenfrequencies $\tilde{\omega}'_n$ of the quadrimer, measured from ω_0, as a function of g, in units of κ. Lower panels: the corresponding imaginary parts of the eigenfrequencies $\tilde{\omega}'_n$. Vertical dashed lines: exceptional points marking broken-unbroken $\mathcal{PT}$ symmetry phases. From left to right along the row of five columns, the second-nearest neighbor coupling constant $h = 0.1\kappa, 0.3\kappa, 0.45\kappa, 0.6\kappa$ and 0.8κ respectively.

A. Tridiagonal matrix

The $\mathcal{PT}$-symmetric mean-field Hamiltonian $\hat{H}'$ of the coupled oligomer chain, for an arbitrary number of oscillators $\mathcal{N}$, has the form [cf. Eq. (10) in the main text]

$$\hat{H}' = \left(\omega_0 + \mathrm{i}\tfrac{\kappa}{2}\right) b_1^\dagger b_1 + \omega_0 \sum_{n=2}^{\mathcal{N}-1} b_n^\dagger b_n + \left(\omega_0 - \mathrm{i}\tfrac{\kappa}{2}\right) b_{\mathcal{N}}^\dagger b_{\mathcal{N}} + g \sum_{n=1}^{\mathcal{N}-1} \left(b_n^\dagger b_{n+1} + b_{n+1}^\dagger b_n\right) . \tag{S23}$$

The effective Hamiltonian of Eq. (S23) has a standard tridiagonal $\mathcal{N} \times \mathcal{N}$ matrix form [cf. Eq. (8) in the main text]

$$\mathcal{H} = \begin{pmatrix} \omega_0 + \mathrm{i}\frac{\kappa}{2} & g & 0 & 0 & \dots & 0 \\ g & \omega_0 & g & 0 & \dots & 0 \\ 0 & g & \omega_0 & g & & 0 \\ \vdots & & \ddots & \ddots & \ddots & \vdots \\ 0 & \dots & 0 & g & \omega_0 & g \\ 0 & \dots & 0 & 0 & g & \omega_0 - \mathrm{i}\frac{\kappa}{2} \end{pmatrix}, \tag{S24}$$

which allows for an analytical treatment due to its simplicity. The Schrödinger equation $\mathcal{H}\hat{\psi} = \varepsilon\hat{\psi}$, for the eigenenergies ε, and within the singly occupied basis $\hat{\psi} = \sum_n c_n b_n^\dagger |\mathbf{0}\rangle$, where $|\mathbf{0}\rangle = |0_1, 0_2, \cdots 0_{\mathcal{N}}\rangle$ is the vacuum state and c_n are coefficients to be found, leads to a recurrence equation in the single excitation sector for the bulk

$$g c_{n-1} + \omega_0 c_n + g c_{n+1} = \varepsilon c_n, \qquad n = 2, 3, ..., \mathcal{N} - 1 \tag{S25}$$

and to two equations describing the edges of the system

$$g c_0 + \left(\omega_0 + \mathrm{i}\tfrac{\kappa}{2}\right) c_1 + g c_2 = \varepsilon c_1, \tag{S26}$$

$$g c_{\mathcal{N}-1} + \left(\omega_0 - \mathrm{i}\tfrac{\kappa}{2}\right) c_{\mathcal{N}} + g c_{\mathcal{N}+1} = \varepsilon c_{\mathcal{N}}. \tag{S27}$$

The matrix Hamiltonian of Eq. (S24) implies the hard-wall boundary conditions $c_0 = c_{\mathcal{N}+1} = 0$, which allows us to treat the eigenvalue problem with the transfer matrix method in a similar manner to the procedures used in Refs. [1, 2].

B. Transfer matrices

The obtained Eq. (S25) and Eq. (S26) are second-order difference equations. However, they can be reduced to first-order difference equations using the framework of transfer matrices [1, 2], thus we introduce

$$C_2 = T_{\mathrm{I}} C_1 \,, \tag{S28}$$

$$C_{n+1} = T_{\mathrm{II}} C_n \,, \qquad n = 2, 3, ..., \mathcal{N} - 1 \tag{S29}$$

$$C_{\mathcal{N}+1} = T_{\mathrm{III}} C_{\mathcal{N}}, \tag{S30}$$

where we define C_n, the two-dimensional column vector, as

$$C_n = \begin{pmatrix} c_{n-1} \\ c_n \end{pmatrix}, \tag{S31}$$

in terms of the coefficients c_n appearing in Eq. (S25) and Eq. (S26). In Eq. (S28), the three transfer matrices are

$$T_{\rm I} = \begin{pmatrix} 0 & 1 \\ -1 & \alpha_{\rm I} \end{pmatrix}, \quad T_{\rm II} = \begin{pmatrix} 0 & 1 \\ -1 & 2\alpha_{\rm II} \end{pmatrix}, \quad T_{\rm III} = \begin{pmatrix} 0 & 1 \\ -1 & \alpha_{\rm III} \end{pmatrix}, \tag{S32}$$

where the factor of 2 in front of $\alpha_{\rm II}$ is convenient for the subsequent recursive treatment, and where

$$\alpha_{\rm I} = \frac{\varepsilon - \omega_0 - {\rm i}\frac{\kappa}{2}}{g}, \quad \alpha_{\rm II} = \frac{\varepsilon - \omega_0}{2g}, \quad \alpha_{\rm III} = \frac{\varepsilon - \omega_0 + {\rm i}\frac{\kappa}{2}}{g}. \tag{S33}$$

The first-order difference equations given by Eq.(S28) and Eq.(S29) and Eq.(S30) can be recursively combined into a single transfer matrix equation

$$C_{\mathcal{N}+1} = \mathbb{T} C_1, \tag{S34}$$

where the 2×2 transfer matrix $\mathbb{T}$ can be expressed as

$$\mathbb{T} = T_{\rm III} T_{\rm II}^{\mathcal{N}-2} T_{\rm I}. \tag{S35}$$

The hard-wall boundary conditions are satisfied if the bottom-right element of $\mathbb{T}$ vanishes, that is $\mathbb{T}_{22} = 0$. This condition provides a secular equation quantizing the eigenenergies ε of the system. In order to find the secular equation we require the powers of the transfer matrix $T_{\rm II}$, which can be readily obtained using Caley-Hamilton theorem, as

$$T_{\rm II}^{\mathcal{N}-2} = \frac{1}{\sin\theta} \begin{pmatrix} -\sin\left[\theta\left(\mathcal{N}-3\right)\right] & \sin\left[\theta\left(\mathcal{N}-2\right)\right] \\ -\sin\left[\theta\left(\mathcal{N}-2\right)\right] & \sin\left[\theta\left(\mathcal{N}-1\right)\right] \end{pmatrix}, \tag{S36}$$

where $\alpha_{\rm II} = \cos\theta$, and so the real eigenenergies ε are parameterized via θ as follows [cf. Eq. (S33)]

$$\varepsilon = \omega_0 + 2g\cos\theta. \tag{S37}$$

Using Eq. (S35) and Eq. (S36), the secular equation $\mathbb{T}_{22} = 0$ reads

$$\frac{1}{\sin\theta}\left\{ \sin\left[\theta\left(\mathcal{N}-3\right)\right] - \left(\alpha_{\rm I} + \alpha_{\rm III}\right)\sin\left[\theta\left(\mathcal{N}-2\right)\right] + \alpha_{\rm I}\alpha_{\rm III}\sin\left[\theta\left(\mathcal{N}-1\right)\right] \right\} = 0, \tag{S38}$$

which may be simplified using $\alpha_{\rm I}\alpha_{\rm III} = 4\cos^2\theta + \kappa^2/(4g^2)$ and $\alpha_{\rm I} + \alpha_{\rm III} = 4\cos\theta$, so that one arrives at a transcendental equation determining the real eigenenergies ε via the parameter θ [cf. Eq. (S37)]

$$\frac{4g^2}{\kappa^2}\sin\left[\theta\left(\mathcal{N}+1\right)\right] + \sin\left[\theta\left(\mathcal{N}-1\right)\right] = 0, \tag{S39}$$

where $0 < \theta < \pi$, since in Eq. (S39) we have removed the $1/\sin\theta$ prefactor from Eq. (S38). In the Hermitian limit of the problem, that is with $\kappa \to 0$, only the first term in Eq. (S39) is relevant, and the zeros of this first sine function, $\sin\left[\theta\left(\mathcal{N}+1\right)\right] = 0$, immediately yield the oligomer eigenfrequencies as given as Eq. (28) in the main text. With nonzero κ, one must solve the full Eq. (S39) in order to obtain the real eigenenergies ε in the unbroken $\mathcal{PT}$-symmetric phase. Notably, this Eq. (S39) is similar to the secular equations derived for graphene nanoribbons with zigzag [1] and bearded edges [3], and as much admits a similar formal analysis.

C. Exceptional points

The locations of the exceptional points in $\mathcal{PT}$-symmetric chains of oscillators correspond to the transitions points linking bulk and edge states in the zigzag and bearded nanoribbons [1, 3], and therefore a similar inspection may be carried out. We are interested in the $\mathcal{N}$ real and distinct roots of Eq. (S39) for a system of size $\mathcal{N}$, which may be found for a certain set ratio of g/κ by modulating θ between 0 and π. The exceptional point for a chain of length $\mathcal{N}$ is revealed by the number of real roots becoming less than $\mathcal{N}$, which implies that the missing solutions correspond to complex roots and thus the broken $\mathcal{PT}$-symmetric phase.

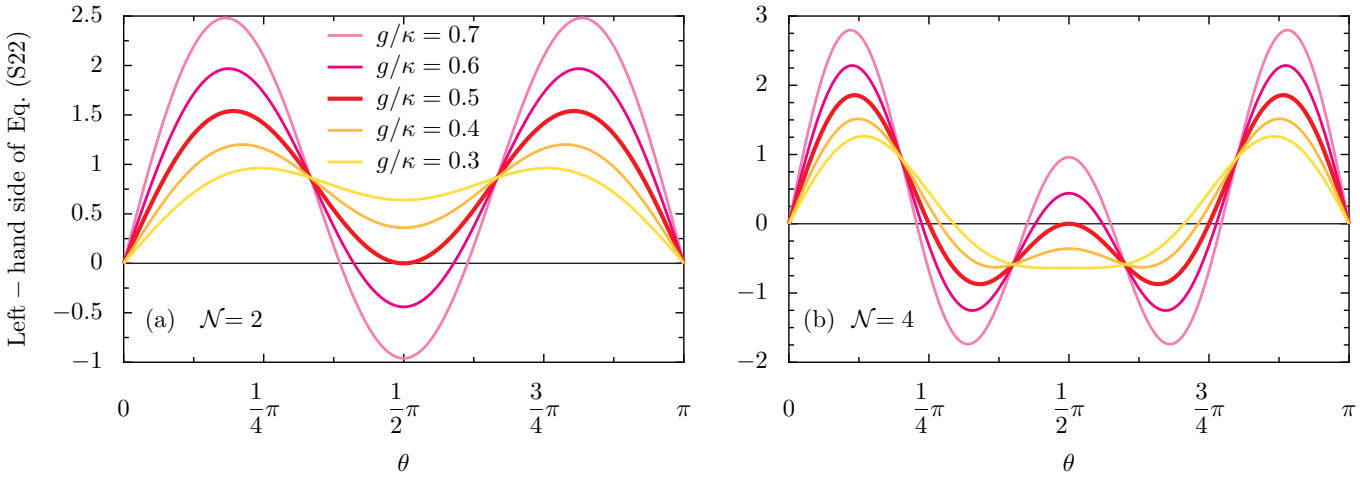

FIG. S7. **Finding roots for oligomers of even $\mathcal{N}$.** Graphical solutions of the transcendental equation given by Eq. (S39), where the real roots are given by the zeros of the left-hand side of the secular Eq. (S39) with $0 < \theta < \pi$, and correspond to the real eigenenergies ε of the oligomer system [cf. Eq. (S37)]. Legend: different ratios of g/κ, where the exceptional point $(g/\kappa)_{\mathcal{N}}$ is given by the thick red line [cf. Eq. (S40)], unbroken $\mathcal{PT}$-symmetric phases are associated with the thin pink lines, and broken $\mathcal{PT}$-symmetric phases are associated with the thin yellow lines. Panel (a): the oligomer is of size $\mathcal{N} = 2$, such that there are 2 real and distinct roots in the unbroken $\mathcal{PT}$-symmetric phase. Panel (b): $\mathcal{N} = 4$.

Let us first consider the case of an even number of oscillators $\mathcal{N} = 2, 4, 6, ...$ in the oligomer. Within the bounds $0 < \theta < \pi$, the second term in Eq. (S39) has a maximum amplitude of unity, which occurs when $\theta = \pi/2$. The maximum amplitude of the first term in Eq. (S39) is $4g^2/\kappa^2$, such that there are only $\mathcal{N}$ real roots when $g/\kappa \leq 1/2$, revealing the exceptional points

$$\left(\frac{g}{\kappa}\right)_{\mathcal{N}} = \frac{1}{2}, \quad \mathcal{N} = 2, 4, 6, ... \tag{S40}$$

which is clearly independent of the even number $\mathcal{N}$. This fact is demonstrated graphically in Fig. S7, where we plot the left-hand side of the secular Eq. (S39) as a function of θ for several different ratios of g/κ. In panel (a) we consider the simplest case of $\mathcal{N} = 2$, where one notices two real and distinct roots for large enough g/κ (thin pink lines), and no roots for too small g/κ (thin yellow lines). The special circumstance of the exceptional point at $g/\kappa = 1/2$ (thick red line) has a repeated root exactly at $\theta = \pi/2$. In panel (b) we represent the next simplest situation, when $\mathcal{N} = 4$. Here familiar features may be found, including cases with four real roots (thin pink lines) and only two real roots (thin yellow lines), with a marginal case of three distinct real roots at the exceptional point (thick red line).

When there are an odd number $\mathcal{N} = 3, 5, 7, ...$ of oscillators in the oligomer the analysis is markedly different. Now it is crucial for the curve associated with the left-hand side of Eq. (S39), plotted as a function of θ, to have a specific sign of gradient at $\theta = \pi/2$ in order to guarantee $\mathcal{N}$ real roots. A Taylor expansion of Eq. (S39) at $\theta = \pi/2 + \delta\theta$ reveals that the gradient is zero when $\mathcal{N} - 1 - 4(\mathcal{N} + 1)g^2/\kappa^2 = 0$, implying the exceptional points

$$\left(\frac{g}{\kappa}\right)_{\mathcal{N}} = \frac{1}{2}\sqrt{\frac{\mathcal{N}-1}{\mathcal{N}+1}}, \quad \mathcal{N} = 3, 5, 7, ... \tag{S41}$$

which quickly approaches $(g/\kappa)_{\mathcal{N}} \simeq (1 - \mathcal{N}^{-1})/2$ with $\mathcal{N} \gg 1$, showcasing an inverse-linear trend towards the asymptotic result of $(g/\kappa)_{\mathcal{N}\to\infty} \to 1/2$. The behavior of the left-hand side of Eq. (S39) for odd $\mathcal{N}$, and especially its roots, is displayed in Fig. S8 [cf. Fig. S7 for the case of even $\mathcal{N}$]. In panel (a), where $\mathcal{N} = 3$, it is most apparent that there are 3 real roots for large g/κ (thin pink lines) and one real root for small g/κ (thin yellow lines), with the crossover occurring at the exceptional point $g/\kappa = 1/(2\sqrt{2}) \simeq 0.353...$ (thick red line). Likewise for $\mathcal{N} = 5$ in panel (b), where the exceptional point $g/\kappa = 1/\sqrt{6} \simeq 0.408...$ marks the transition from 5 to 3 real roots.

D. Complex eigenenergies

The framework of Sec. III B, cumulating in Eq. (S39) with the parameterization Eq. (S37), captures the real eigenenergies of the oligomer corresponding to the unbroken $\mathcal{PT}$-symmetric phase. The onset of the broken $\mathcal{PT}$-symmetric phase is marked by the exceptional points of Eq. (S40) and Eq. (S41), above which the eigenenergies acquire imaginary parts. In order to find these

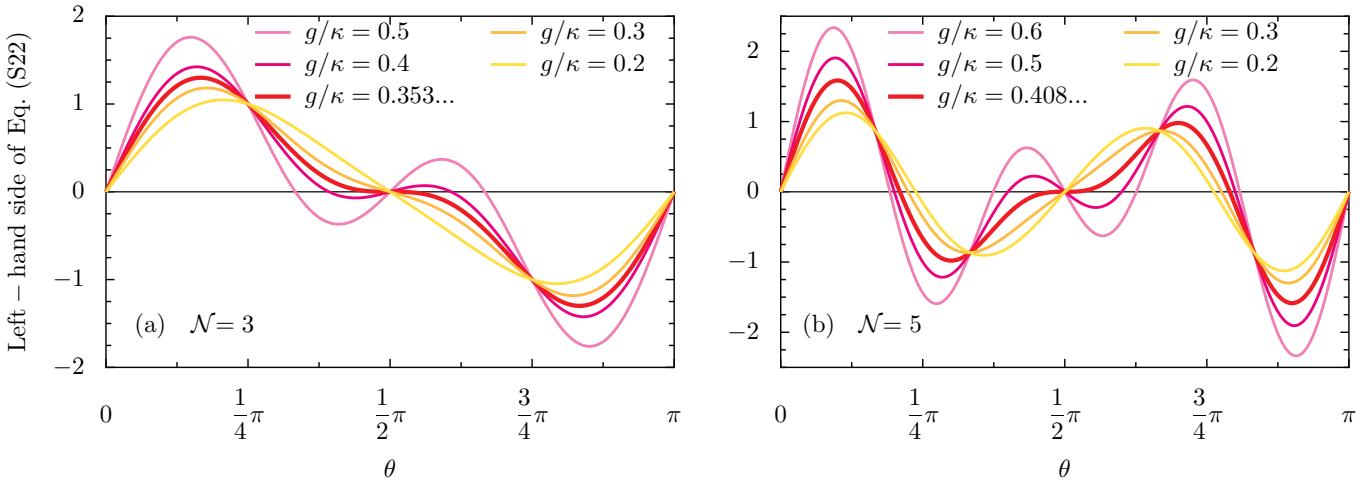

FIG. S8. **Finding roots for oligomers of odd $\mathcal{N}$.** Graphical solutions of the transcendental equation given by Eq. (S39), where the real roots are given by the zeros of the left-hand side of the secular Eq. (S39) with $0 < \theta < \pi$, and correspond to the real eigenenergies ε of the oligomer system [cf. Eq. (S37)]. Legend: different ratios of g/κ, where the exceptional point $(g/\kappa)_{\mathcal{N}}$ is given by the thick red line [cf. Eq. (S41)], unbroken $\mathcal{PT}$-symmetric phases are associated with the thin pink lines, and broken $\mathcal{PT}$-symmetric phases are associated with the thin yellow lines. Panel (a): the oligomer is of size $\mathcal{N} = 3$, such that there are 3 real and distinct roots in the unbroken $\mathcal{PT}$-symmetric phase. Panel (b): $\mathcal{N} = 5$.

complex eigenenergies, one needs to introduce an analytic continuation for the parameter θ appearing in the secular Eq. (S39), using the replacement $\theta = \pi/2 - \mathrm{i}\vartheta$. This procedure leads to two transcendental equations for the complex eigenenergies depending on the parity of the oligomer [cf. Eq. (S39)]

$$\frac{4g^2}{\kappa^2}\cosh\left[\vartheta\left(N+1\right)\right] - \cosh\left[\vartheta\left(N-1\right)\right] = 0, \qquad \mathcal{N} = 2, 4, 6, ... \tag{S42}$$

$$\frac{4g^2}{\kappa^2}\sinh\left[\vartheta\left(N+1\right)\right] - \sinh\left[\vartheta\left(N-1\right)\right] = 0, \qquad \mathcal{N} = 3, 5, 7, ... \tag{S43}$$

where the eigenenergies follow from the re-parameterization [cf. Eq. (S37)]

$$\varepsilon = \omega_0 + 2\mathrm{i}g\sinh\vartheta. \tag{S44}$$

This analysis reveals that the two complex eigenenergies are pinned at the single oscillator resonance frequency ω_0, with a lifetime associated with the imaginary part $2g\sinh\vartheta$. If $\vartheta = x$ is a solution of the transcendental equation then $-x$ is also a solution, so that the pair of complex eigenfrequencies are symmetric with energies $\varepsilon = \omega_0 \pm 2\mathrm{i}g\sinh x$. When considering chains of an odd parity $\mathcal{N} = 3, 5, 7, ...$ we can see that Eq. (S43) always admits a solution at $\vartheta = 0$ [as does Eq. (S39) at $\theta = \pi/2$] so that there is always a solution with the eigenfrequency $\varepsilon = \omega_0$. This is not the case for chains of an even parity, where there is no simple ω_0 solution [cf. Eq. (S42)].

We can visualize some general properties of $\mathcal{PT}$-symmetric oligomers by looking at Fig. S9. In this figure, we show the real and imaginary parts of the eigenfrequencies $\varepsilon = \omega_n'$ of the $\mathcal{PT}$-symmetric chain in the left column and right column respectively. The $\mathcal{N}$ different line styles correspond to the eigenfrequencies labelled by $n = 1, 2, ..., \mathcal{N}$. Upon descending the columns in Fig. S9, we increase the chain size from $\mathcal{N} = 2$ (pink lines) to 3 (cyan) to 4 (orange) to 5 (green). When considering the even chains $\mathcal{N} = 2$ (first row) and $\mathcal{N} = 4$ (third row), it is noticeable that it is the two eigenfrequencies which are closest to the resonance frequency of a single oscillator ω_0 which become complex below the exceptional point, ensuring 2nd order exceptional points. For typical odd chains, like for the cases $\mathcal{N} = 3$ (second row) and $\mathcal{N} = 5$ (fourth row), apart from the guaranteed eigenfrequency pinned at ω_0, the next two closest eigenfrequencies to ω_0 transition into complex quantities beyond the exceptional point such that the exceptional points are of a higher (3rd) order. These features are characteristic of the $\mathcal{PT}$-symmetric oligomers under investigation.

Supplementary References

[1] V. A. Saroka, M. V. Shuba, and M. E. Portnoi, Optical selection rules of zigzag graphene nanoribbons, Phys. Rev. B **95**, 155438 (2017).
[2] V. A. Saroka, Analytical solutions for energies and wave functions of two coupled quantum rings in tight-binding model, Actual Probl. Radiophys. Proc. VII Int. Conf. "APR-2017", Tomsk. Russ. Sept. 18-22, 2017, pages 5-9, London, 2018. Red Square Scientific.
[3] D. J. Klein, Graphitic polymer strips with edge states, Chem. Phys. Lett. **217**, 261 (1994).

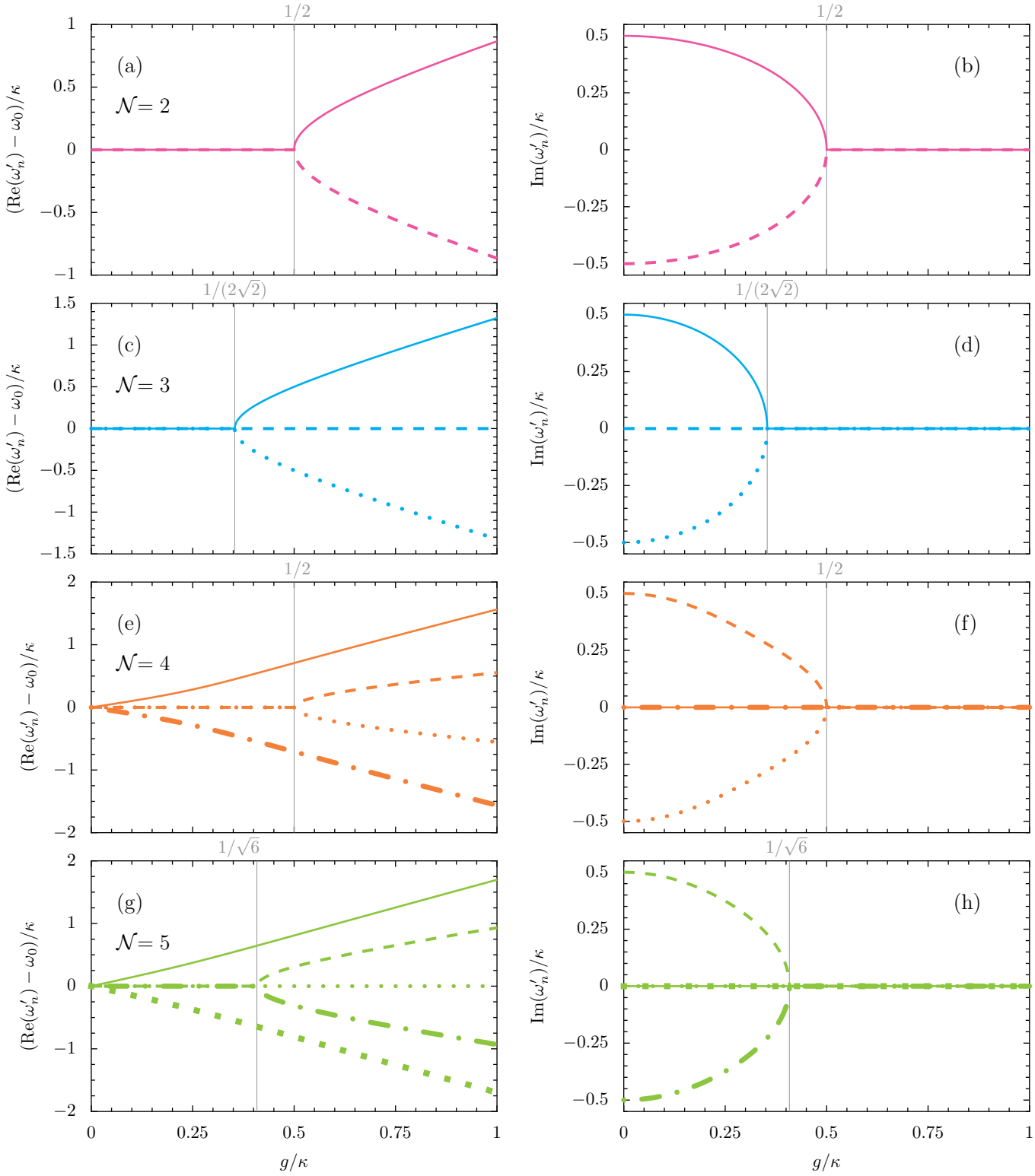

FIG. S9. **Visualizing the exceptional points of oligomers.** Eigenfrequencies ω_n' of the $\mathcal{PT}$-symmetric oligomer chain, where each oscillator is of resonance frequency ω_0, and the coupling constant is g. The first oscillator is subject to gain κ, and the final oscillator to an equivalent loss κ. The $\mathcal{N}$ different line styles correspond to the eigenfrequencies labelled by $n = 1, 2, ..., \mathcal{N}$. Left column: the real parts of the eigenfrequencies ω_n', measured from ω_0, as a function of g, in units of κ. Right column: the corresponding imaginary parts of the eigenfrequencies ω_n'. Thin gray lines: exceptional points marking broken-unbroken $\mathcal{PT}$-symmetric phases [cf. Eq. (S40) and Eq. (S41)]. Upon descending the columns, we increase the chain size from $\mathcal{N} = 2$ (pink lines) to 3 (cyan) to 4 (orange) to 5 (green).